

Supplement of “Predicting the mineral composition of dust aerosols. Part 1: Representing key processes” by Perlwitz et al.

Contents

1	Volume Size Distribution of Minerals at Tinfou, Morocco	S2
5	2 Supplementary Figures	S4
	3 Supplementary Tables	S21

List of Figures

10	S1 Quartz and carbonates at emission	S4
	S2 Illite and kaolinite at emission	S5
	S3 Feldspar, gypsum, and iron oxides at emission	S6
	S4 Global annual mineral wet deposition (Tg).	S7
	S5 Global annual mineral gravitational deposition (Tg).	S8
	S6 Global annual mineral dry turbulent deposition (Tg).	S9
	S7 Global annual mineral emission fractions (%).	S10
15	S8 Global annual mineral mass load fractions (%).	S11
	S9 Global annual mineral wet deposition fractions (%).	S12
	S10 Global annual mineral gravitational deposition fractions (%).	S13
	S11 Global annual mineral dry turbulent deposition fractions (%).	S14
	S12 Total mineral life time (d).	S15
20	S13 Mineral wet deposition life time (d).	S16
	S14 Mineral gravitational deposition life time (d).	S17
	S15 Mineral turbulent deposition life time (d).	S18
	S16 Iron oxides in SMF simulation and SMF noClayFe simulation . . .	S19
	S17 Iron oxides in AMF simulation and AMF noFeAcc simulation . . .	S20

25 List of Tables

S1	Dust cycle statistics from SMF and AMF simulation	S21
----	---	-----

1 Volume Size Distribution of Minerals at Tinfou, Morocco

The normalized volume size distributions in Perlitz et al. (2015, Fig.1) for the minerals were calculated from the relative volume fractions of the minerals (Kandler et al., 2009, Table 1) and the fitted number size distribution (Kandler et al., 2009, Table 4) as follows:

The number density distribution is the sum over four size modes, as the best fit of measured data, each of them follows a log-normal density distribution:

$$\frac{dn}{d\log D} = \frac{\ln 10}{\sqrt{2\pi}} \sum_{i=1}^4 \frac{n_i}{\ln \zeta_i} \exp\left(-\frac{\ln^2(D \cdot m_i^{-1})}{2\ln^2 \zeta_i}\right) \quad (\text{S1})$$

with i is the number of the mode, D is the particle diameter and n_i , m_i and ζ_i , the total number of particles, the number median diameter, and the geometric standard deviation of the i -th mode, respectively.

Using $\log D = \log e \cdot \ln D$ and $\ln 10 = \frac{\log 10}{\log e} = \frac{1}{\log e}$, Eq. (S1) can be rewritten into:

$$\frac{dn}{d\ln D} = \frac{1}{\sqrt{2\pi}} \sum_{i=1}^4 \frac{n_i}{\ln \zeta_i} \exp\left(-\frac{\ln^2(D \cdot m_i^{-1})}{2\ln^2 \zeta_i}\right) \quad (\text{S2})$$

When the number density distribution is log-normally distributed the volume density distribution will be log-normally distributed as well. Both distributions have the same geometric standard deviation. The volume median diameter $m_{V,i}$ and the number median diameter obey to the relationship (Seinfeld and Pandis, 1998, p. 425f),

$$\ln m_{V,i} = \ln m_i + 3\ln^2 \zeta_i \quad (\text{S3})$$

Thus, the density distribution of the particle volume V can be written with the parameters of the number density distribution,

$$\frac{dV}{d\ln D} = \frac{1}{\sqrt{2\pi}} \sum_{i=1}^4 \frac{n_i}{\ln \zeta_i} \exp(3\ln m_i + \frac{9}{2}\ln^2 \zeta_i) \exp\left(-\frac{[\ln D - (\ln m_i + 3\ln^2 \zeta_i)]^2}{2\ln^2 \zeta_i}\right) \quad (\text{S4})$$

With

$$t = \frac{[\ln D - (\ln m_i + 3\ln^2 \zeta_i)]}{\sqrt{2\ln \zeta_i}} \quad (\text{S5})$$

and

$$dt = \frac{1}{\sqrt{2\ln \zeta_i}} d\ln D \quad (\text{S6})$$

we obtain,

$$dV = \frac{1}{2} \sum_{i=1}^4 n_i \exp\left(3 \ln m_i + \frac{9}{2} \ln^2 \zeta_i\right) \frac{2}{\sqrt{\pi}} \exp(-t^2) d \ln t \quad (S7)$$

The volume increment ΔV^k of size bin k is the integral between the lower and
55 upper boundary, D_1^k and D_2^k , of the size bin, respectively,

$$\Delta V^k = \frac{1}{2} \sum_{i=1}^4 n_i \exp\left(3 \ln m_i + \frac{9}{2} \ln^2 \zeta_i\right) (\text{erf}(t_2^k) - \text{erf}(t_1^k)) \quad (S8)$$

where erf is the error function, and t_1^k and t_2^k are related to D_1^k and D_2^k through Eq. (S5).

By multiplying Eq. (S8) with the relative volume fraction v_n^k and normalizing
60 over the total volume of the mineral summed up to a particle size bin K , we obtain a normalized distribution of the volume fractions V_n^k of the mineral phases in dust aerosols over the particle size for each mineral phase n ,

$$\Delta V_n^k = \frac{v_n^k \Delta V^k}{\sum_{k=1}^K v_n^k \Delta V^k} \quad (S9)$$

For the Aerosol Mineral Fraction (AMF) method, the derived volume increments
65 for each mineral, normalized over the size range 2 to 50 μm , were used to partition the mineral masses among the silt size classes of ModelE2. For the Soil Mineral Fraction (SMF) method, the average of the volume increments in each size class, normalized over the size range 2 to 50 μm , was used to partition the mineral masses among the silt size classes.

70 2 Supplementary Figures

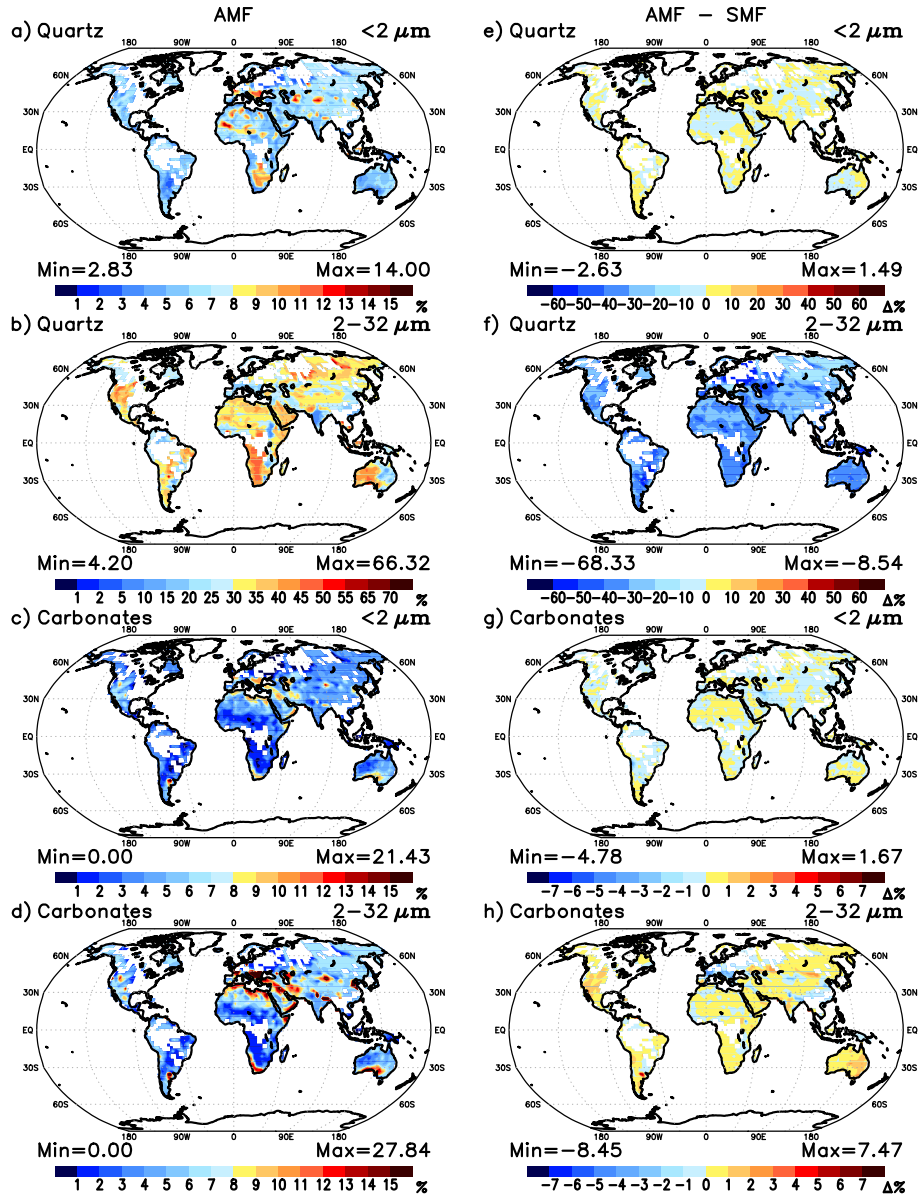


Figure S1. (Left panels) (a, b) Quartz and (c, d) carbonate fractions at emission after reaggregation and fragmentation for the aerosol fraction method (AMF) method, but without additional constraints on emission, for (a, c) the clay-size range and (b, d) the silt-size range at the model resolution of $2^\circ \times 2.5^\circ$ latitude by longitude. (Right panels) Difference of the (e, f) quartz and (g, h) carbonate fractions between AMF method and soil mineral fraction (SMF) method for (e, g) the clay-size range and (f, h) the silt-size range.

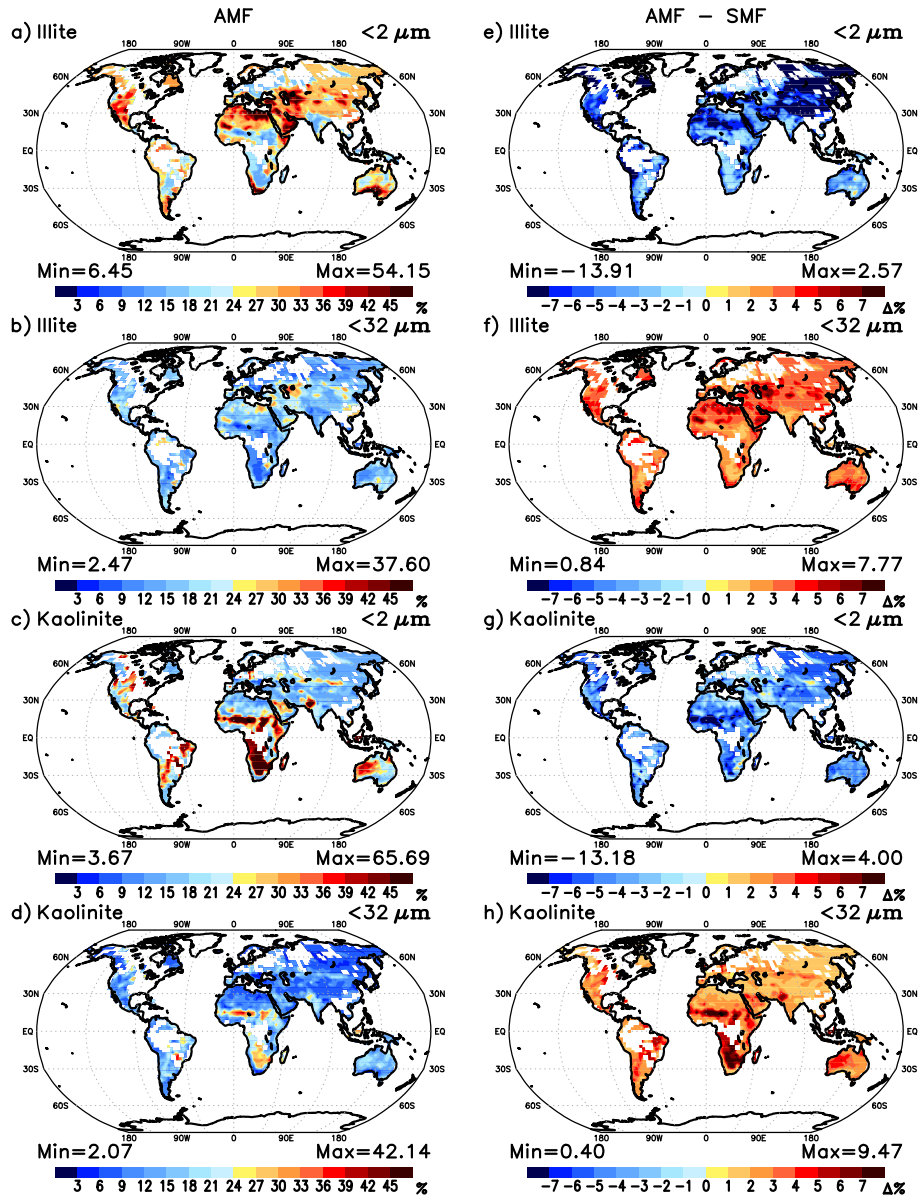


Figure S2. (Left panels) (a, b) Illite and (c, d) kaolinite fractions at emission after reaggregation and fragmentation for the aerosol fraction method (AMF) method, but without additional constraints on emission, for (a, c) the clay-size range and (b, d) the total size range at the model resolution of $2^\circ \times 2.5^\circ$ latitude by longitude. (Right panels) Difference of the (e, f) illite and (g, h) kaolinite fractions between AMF method and soil mineral fraction (SMF) method for (e, g) the clay-size range and (f, h) the total size range.

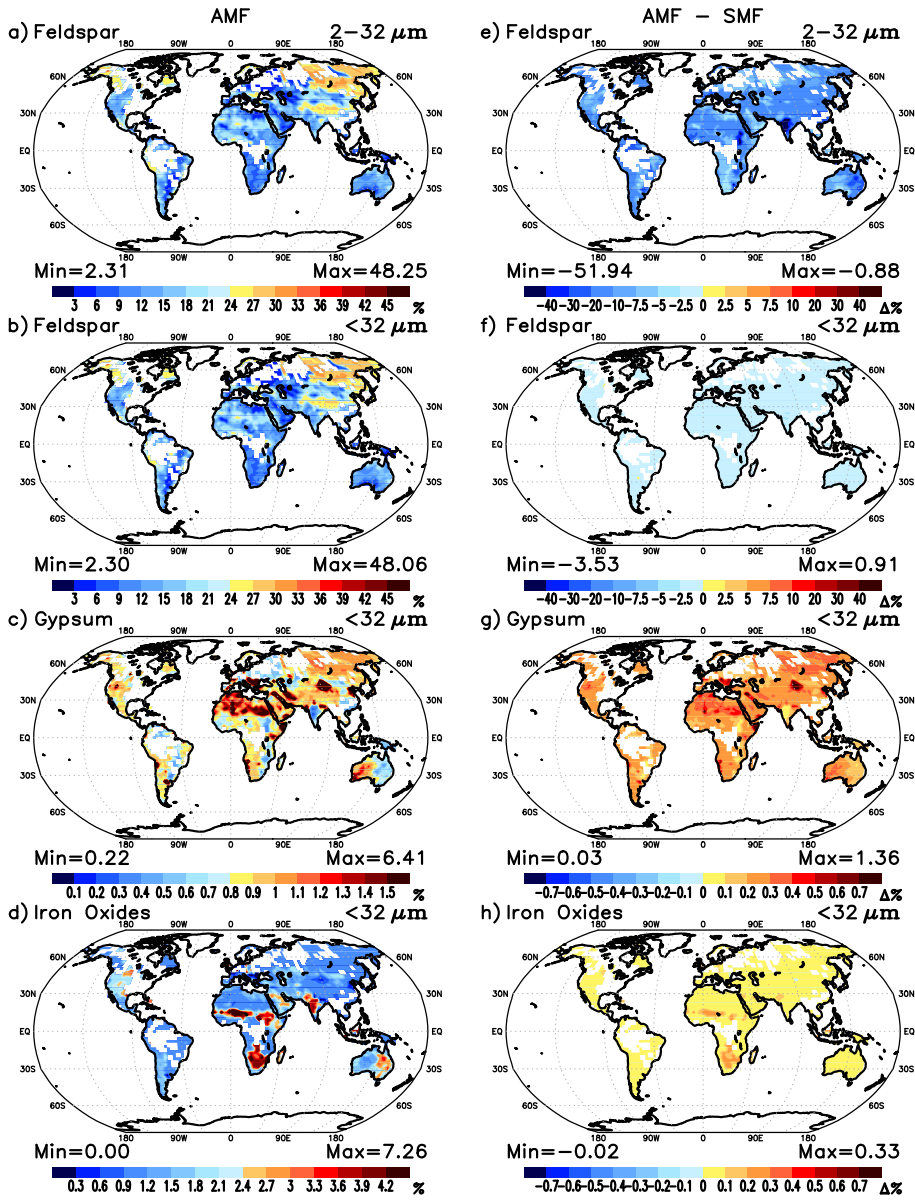


Figure S3. (Left panels) (a, b) Feldspar, (c) gypsum, and (d) iron oxide fractions at emission after reaggregation and fragmentation for the aerosol fraction method (AMF) method, but without additional constraints on emission, for (a) the clay-size range and (b, c, d) the total size range at the model resolution of $2^\circ \times 2.5^\circ$ latitude by longitude. (Right panels) Difference of the (e, f) feldspar, (g) gypsum, and (h) iron oxide fractions between AMF method and soil mineral fraction (SMF) method for (e) the clay-size range and (f, g, h) the total size range.

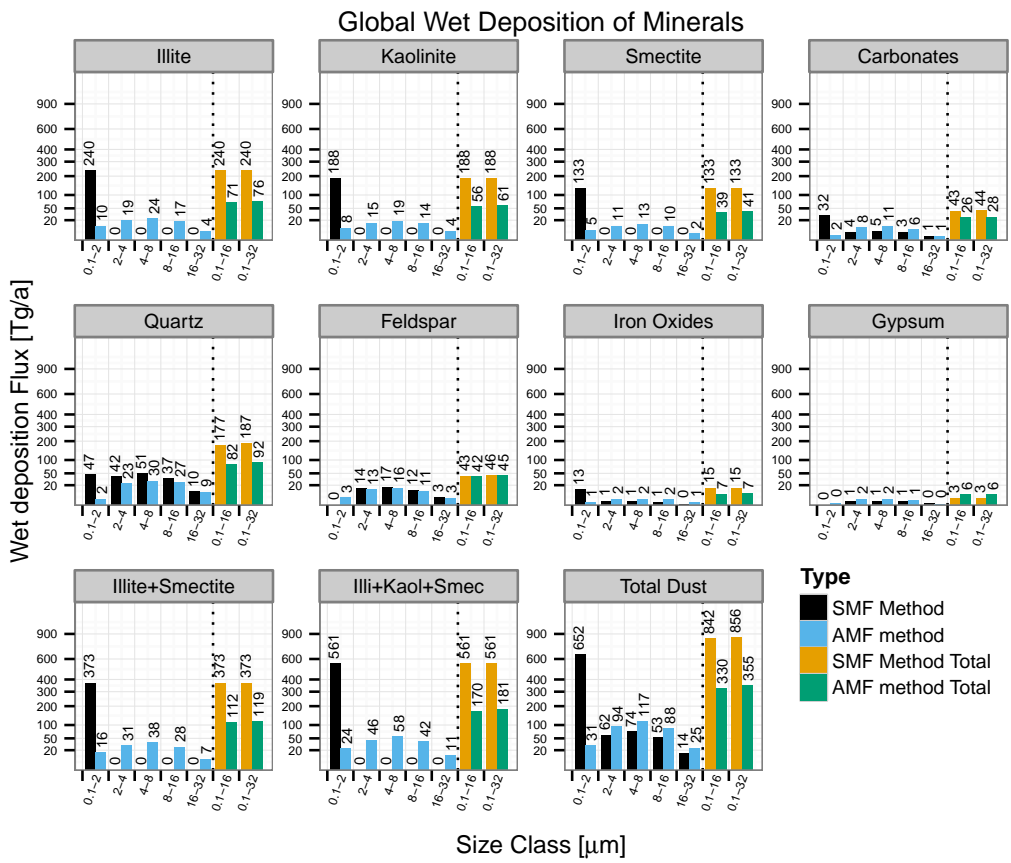


Figure S4. Global annual mineral wet deposition (Tg).

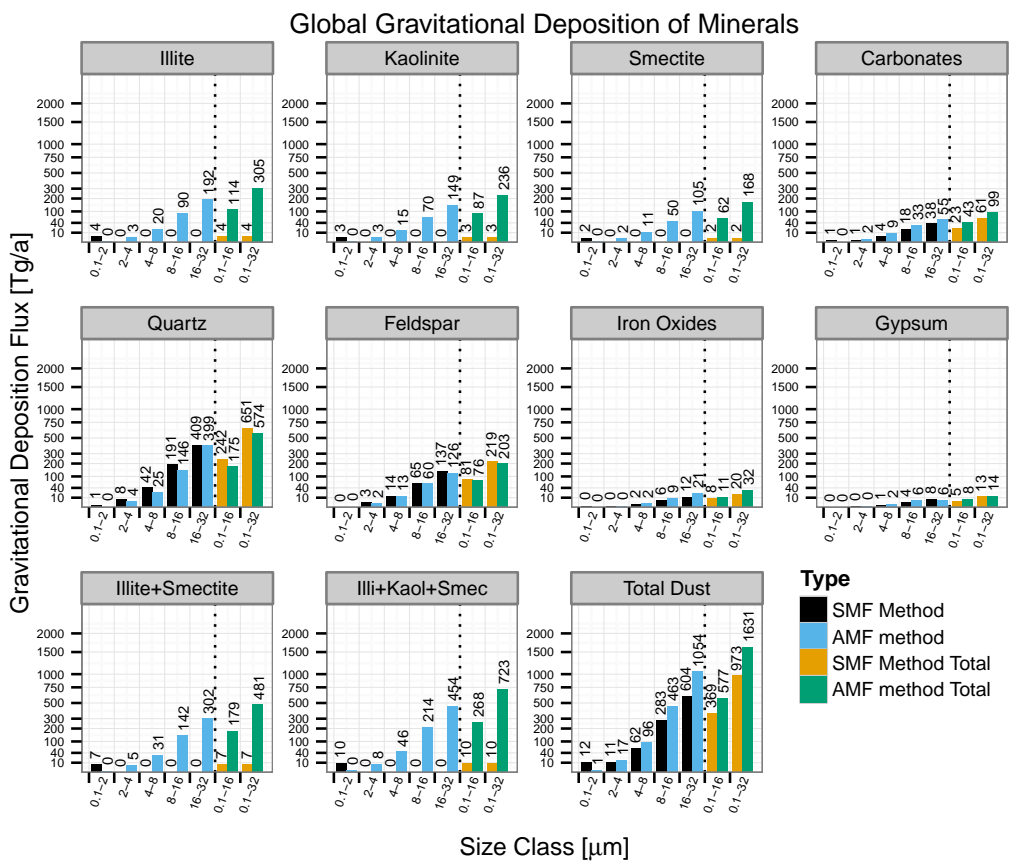


Figure S5. Global annual mineral gravitational deposition (Tg).

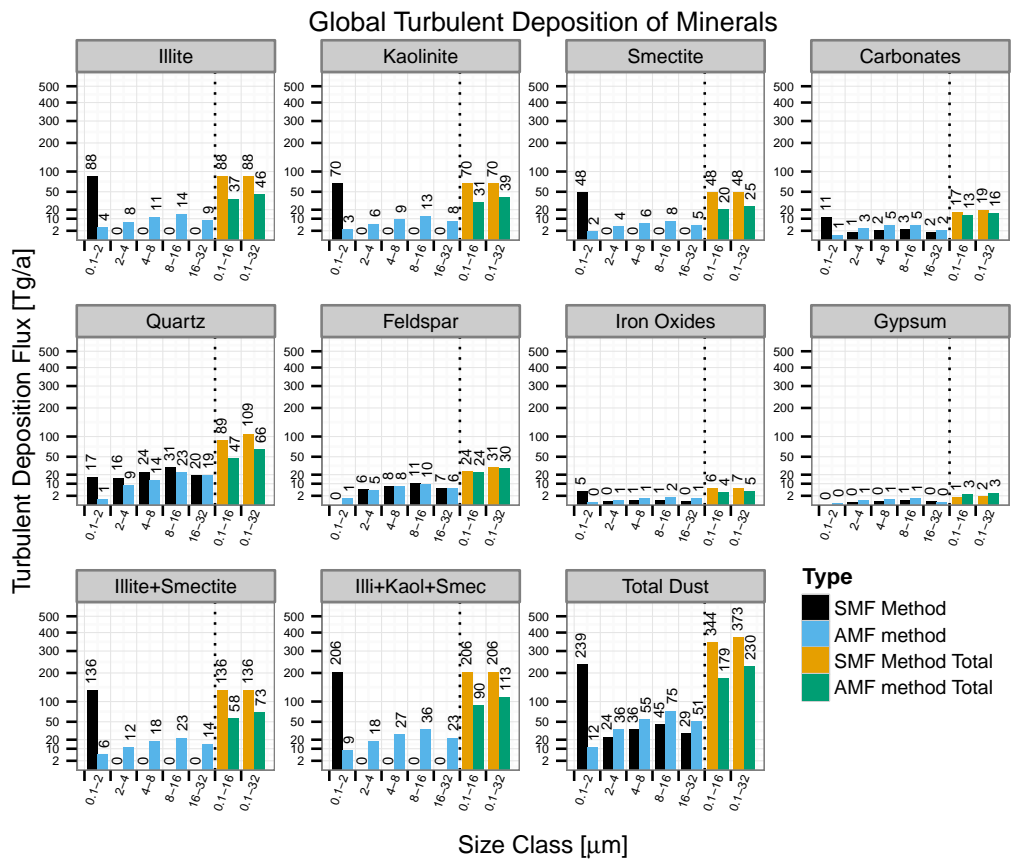


Figure S6. Global annual mineral dry turbulent deposition (Tg).

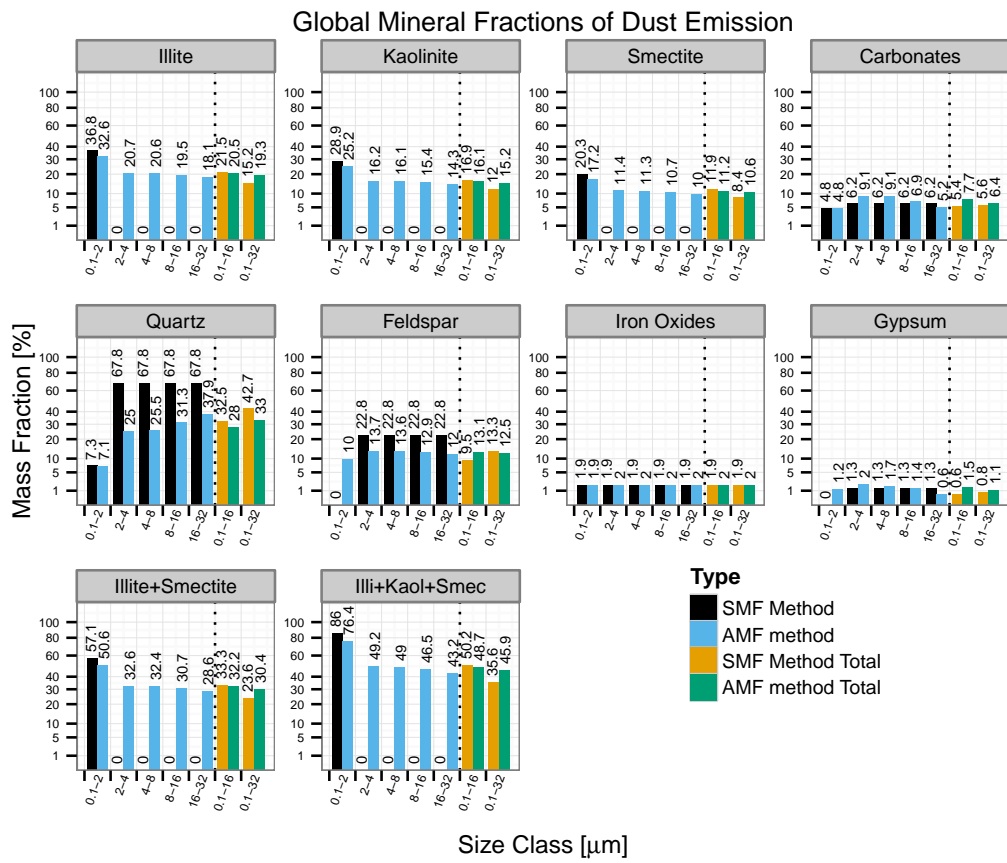


Figure S7. Global annual mineral emission fractions (%).

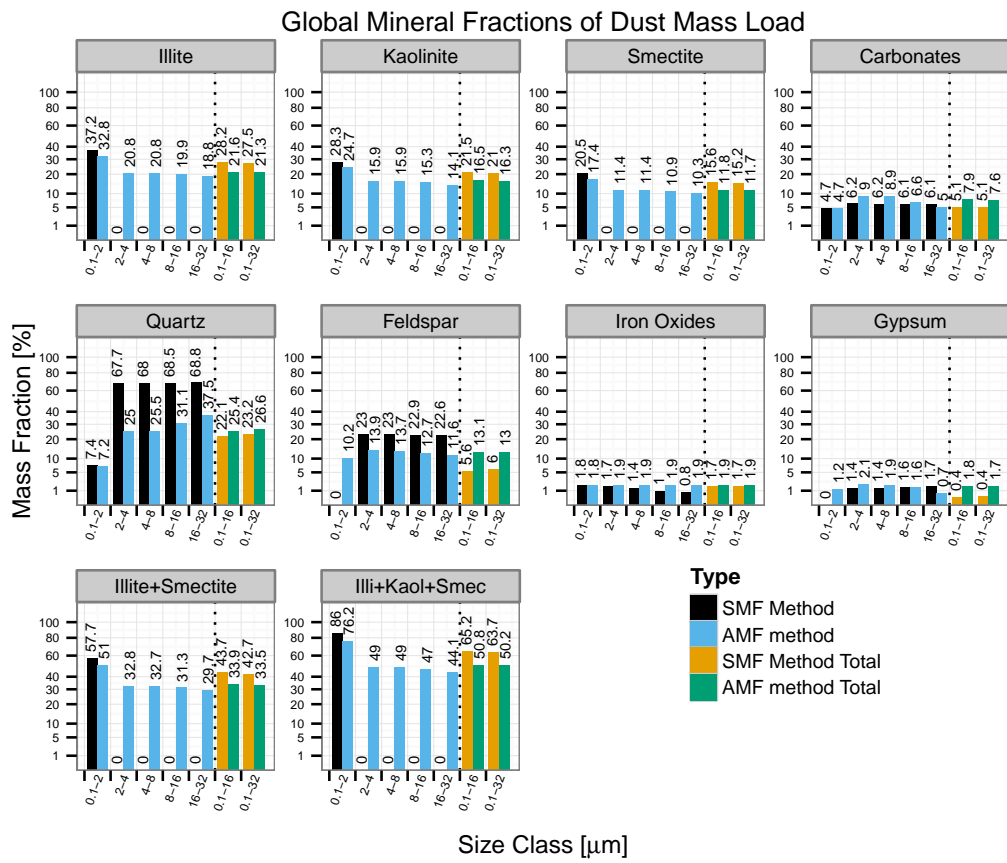


Figure S8. Global annual mineral mass load fractions (%).

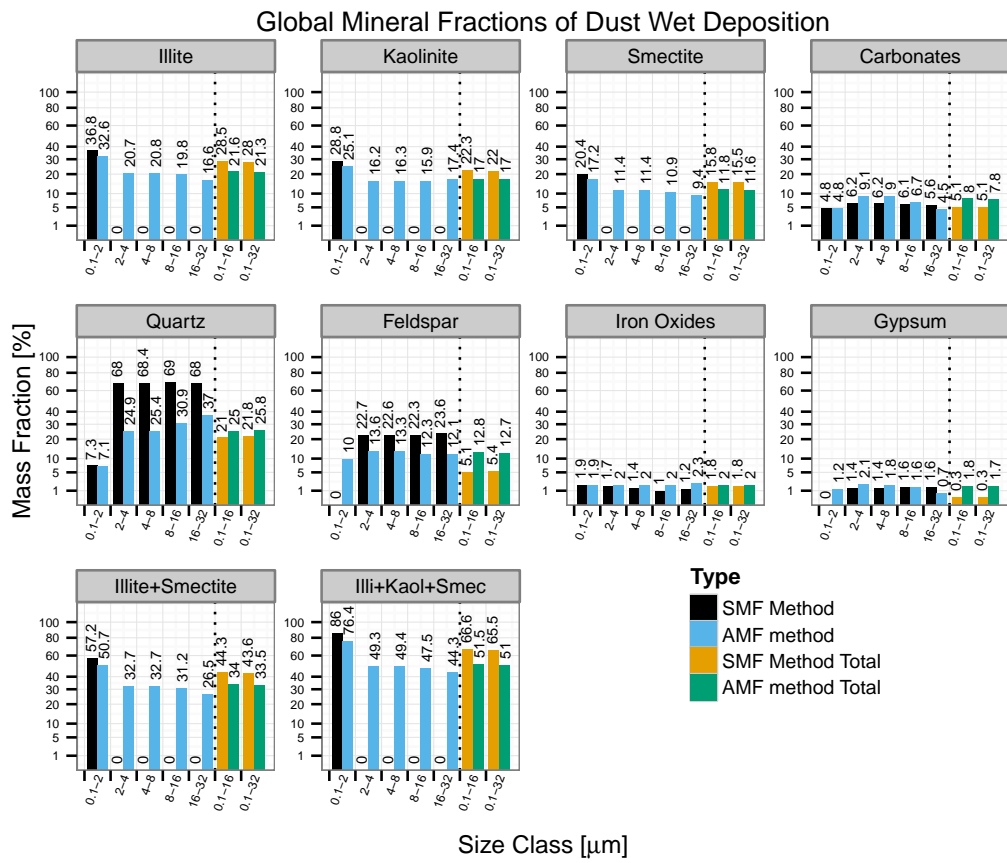


Figure S9. Global annual mineral wet deposition fractions (%).

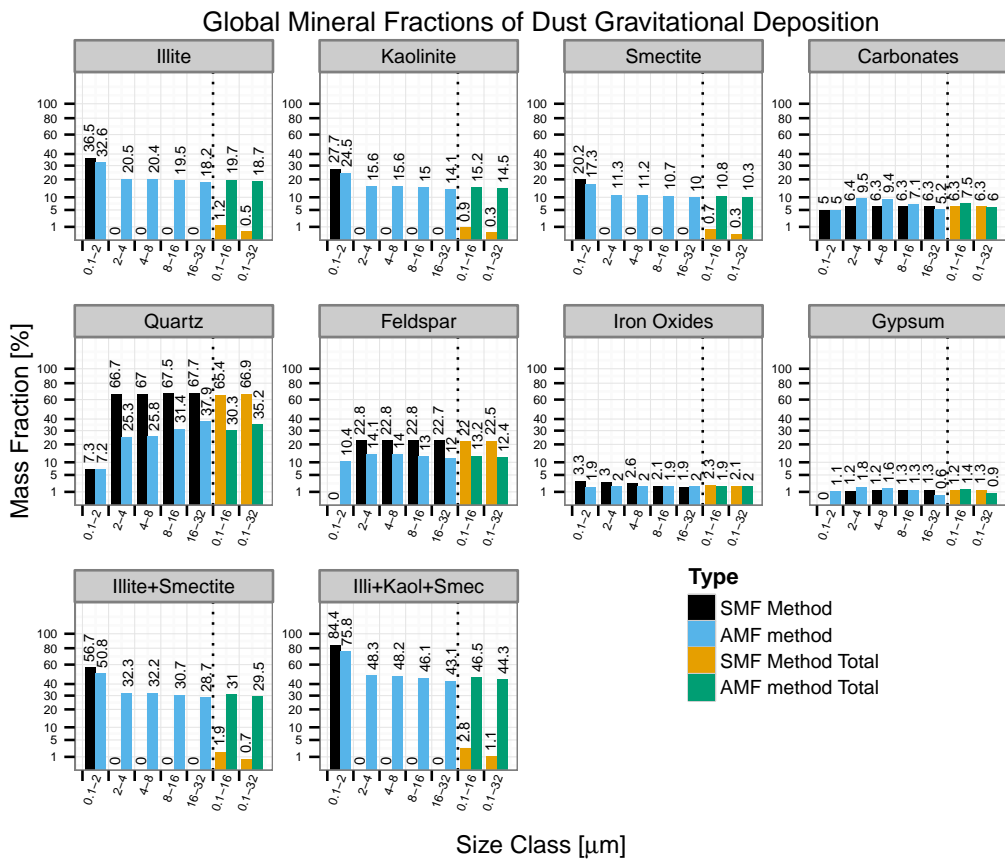


Figure S10. Global annual mineral gravitational deposition fractions (%).

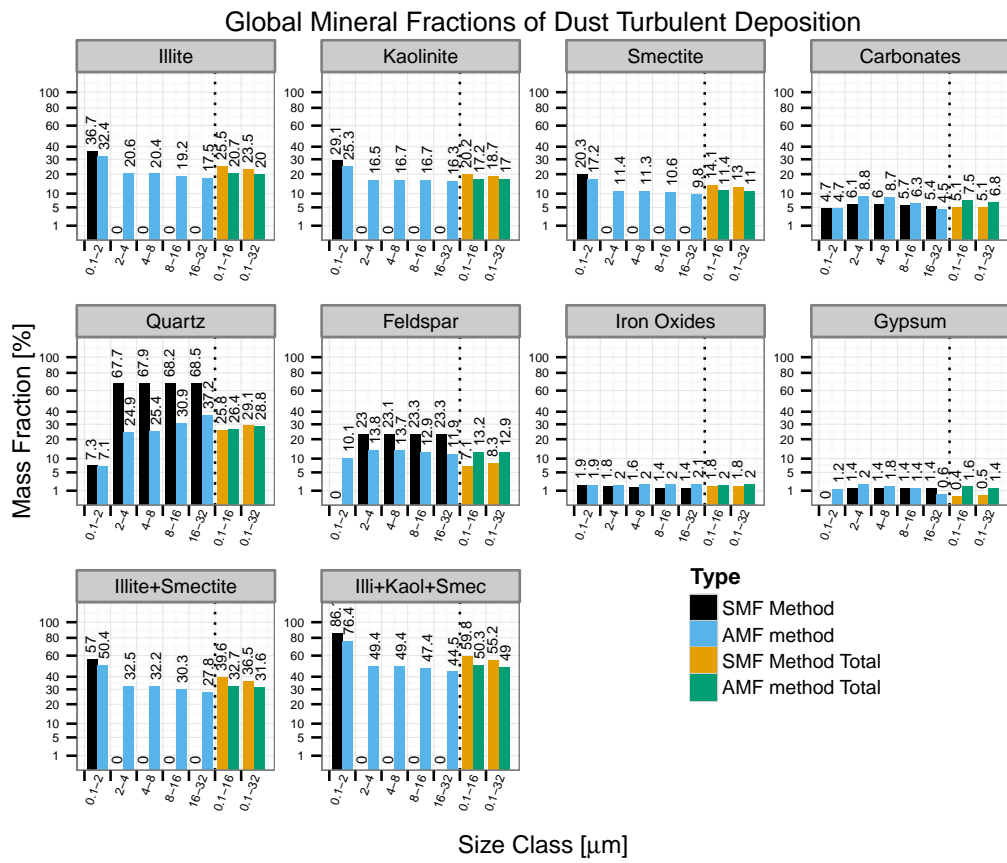


Figure S11. Global annual mineral dry turbulent deposition fractions (%).

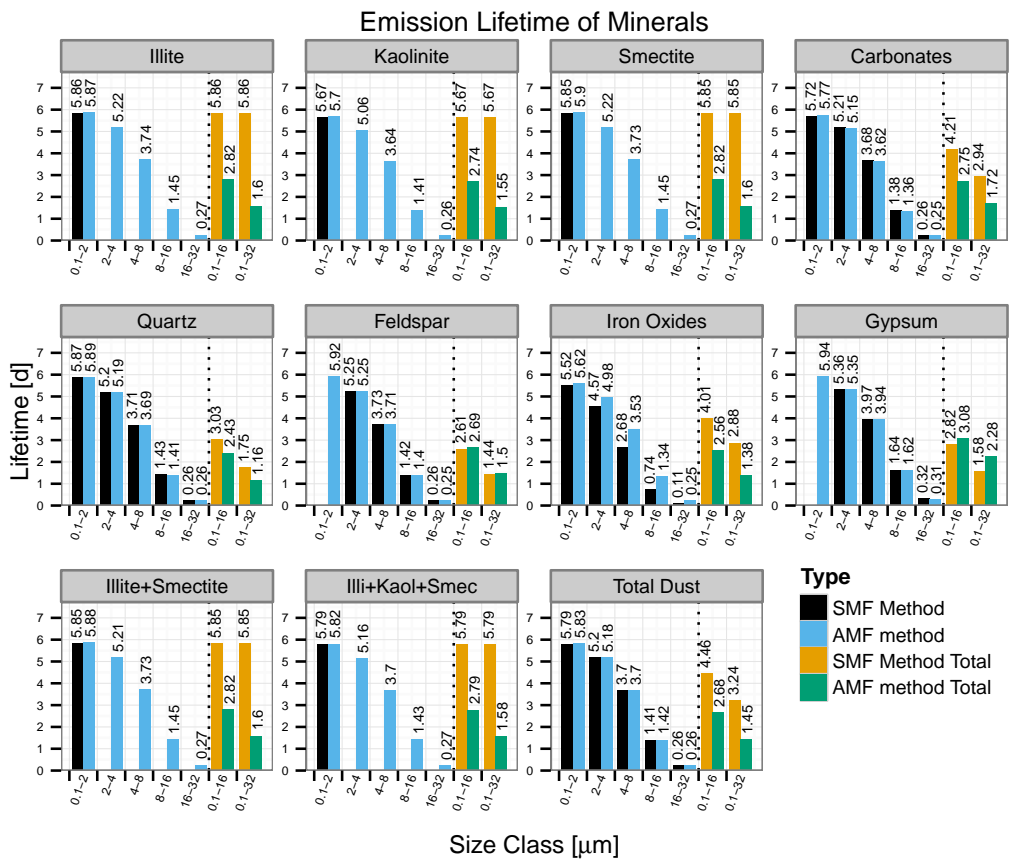


Figure S12. Total mineral life time (d).

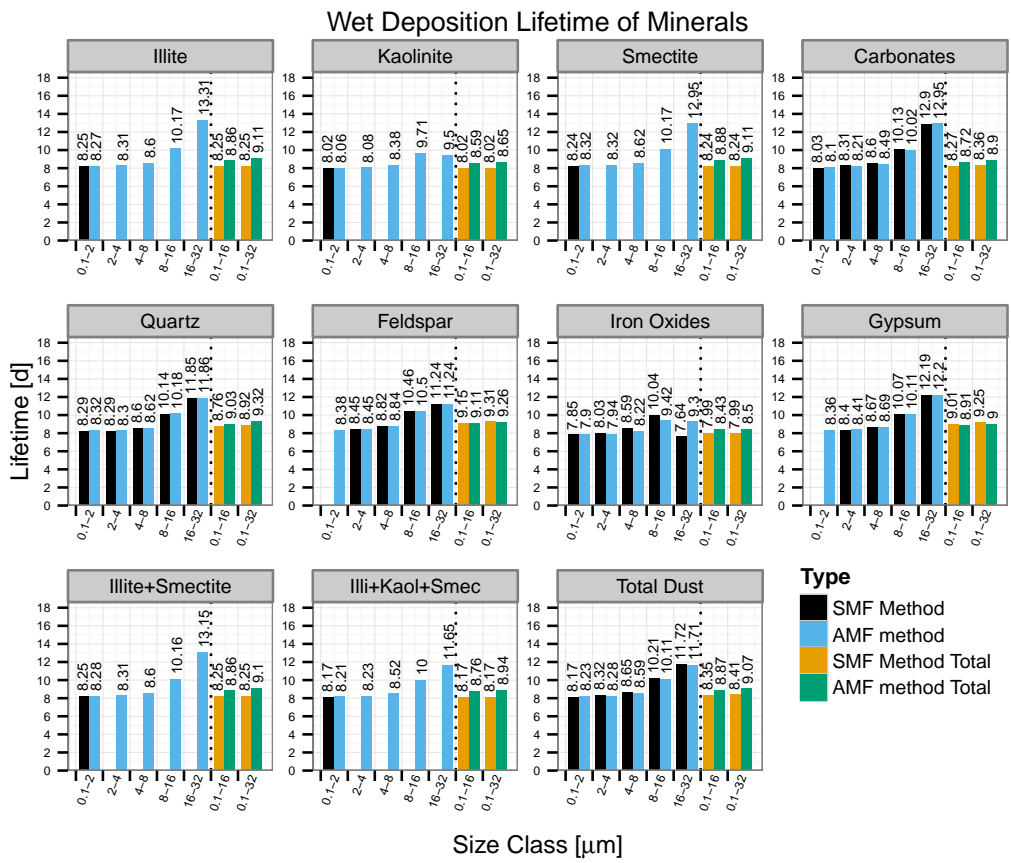


Figure S13. Mineral wet deposition life time (d).

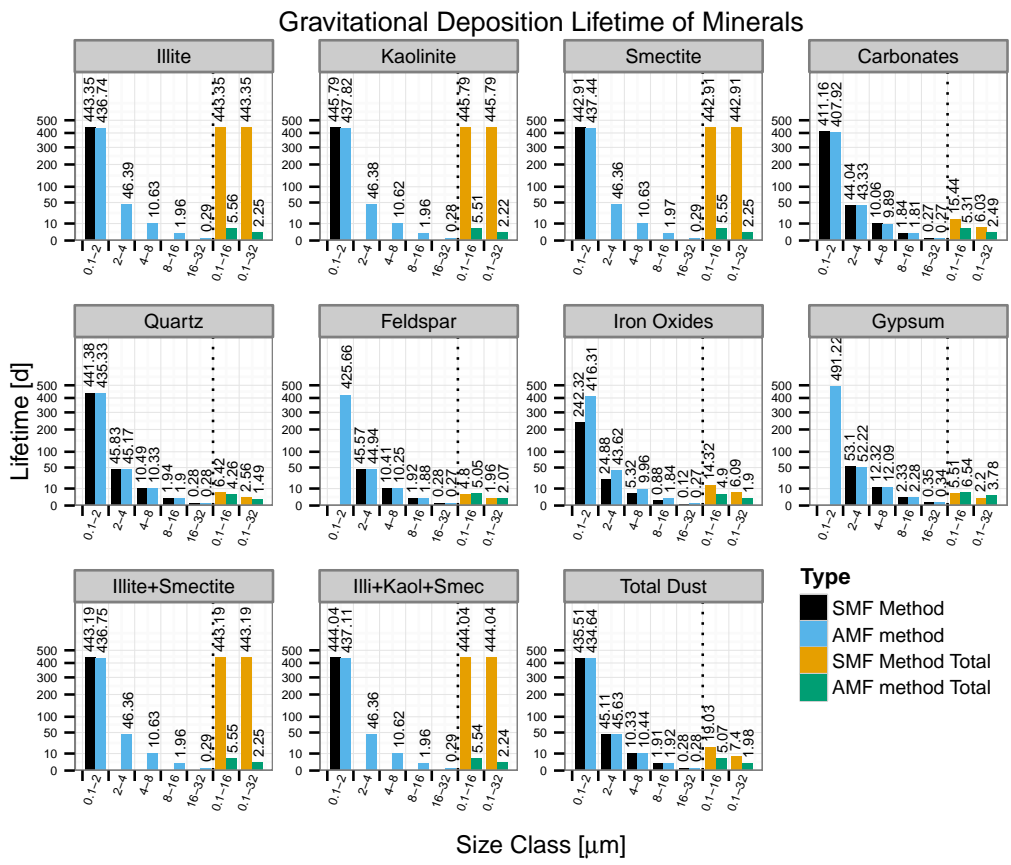


Figure S14. Mineral gravitational deposition life time (d).

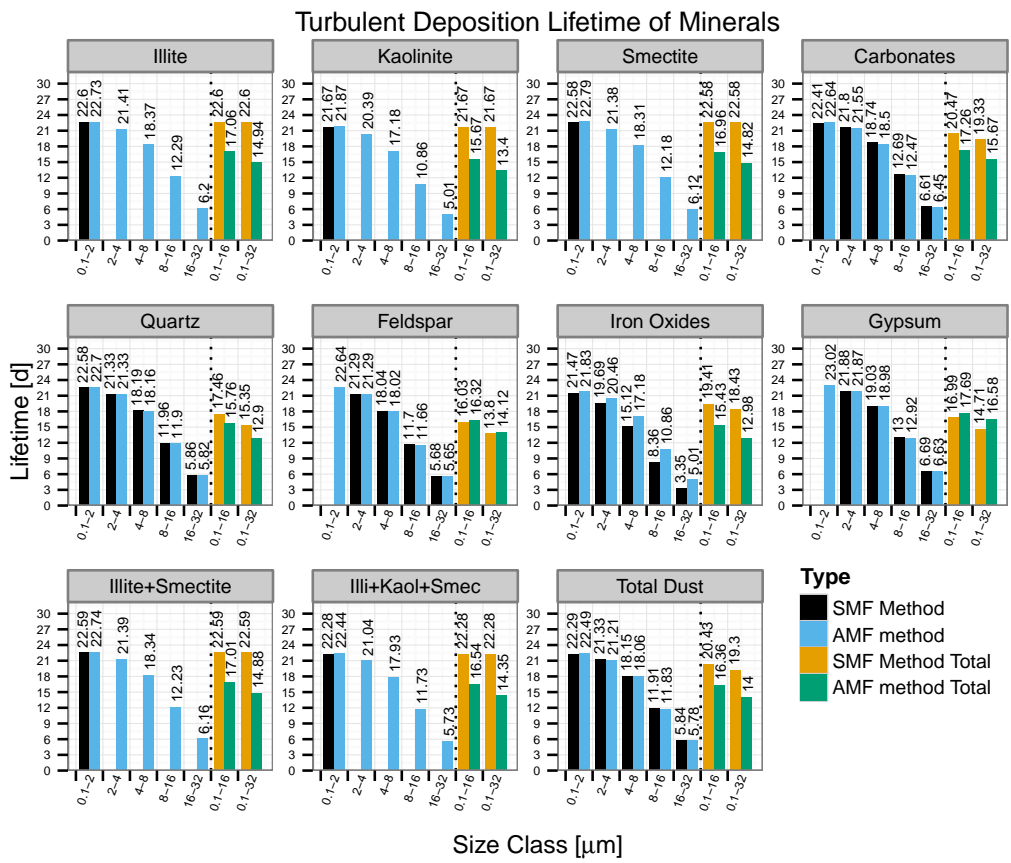


Figure S15. Mineral turbulent deposition life time (d).

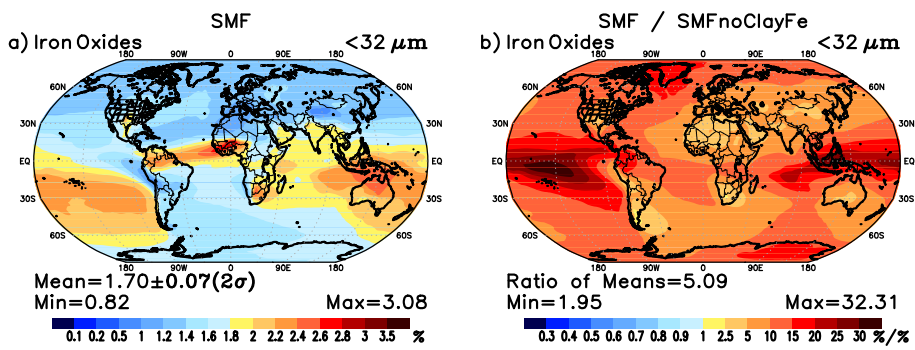


Figure S16. (a) Annual-averae column mass fractions of iron oxides for the soil mineral fraction (SMF) method and (b) column mass fraction ratios between the SMF method and the SMF method without iron oxides (SMF-noClayFe) in the clay size range.

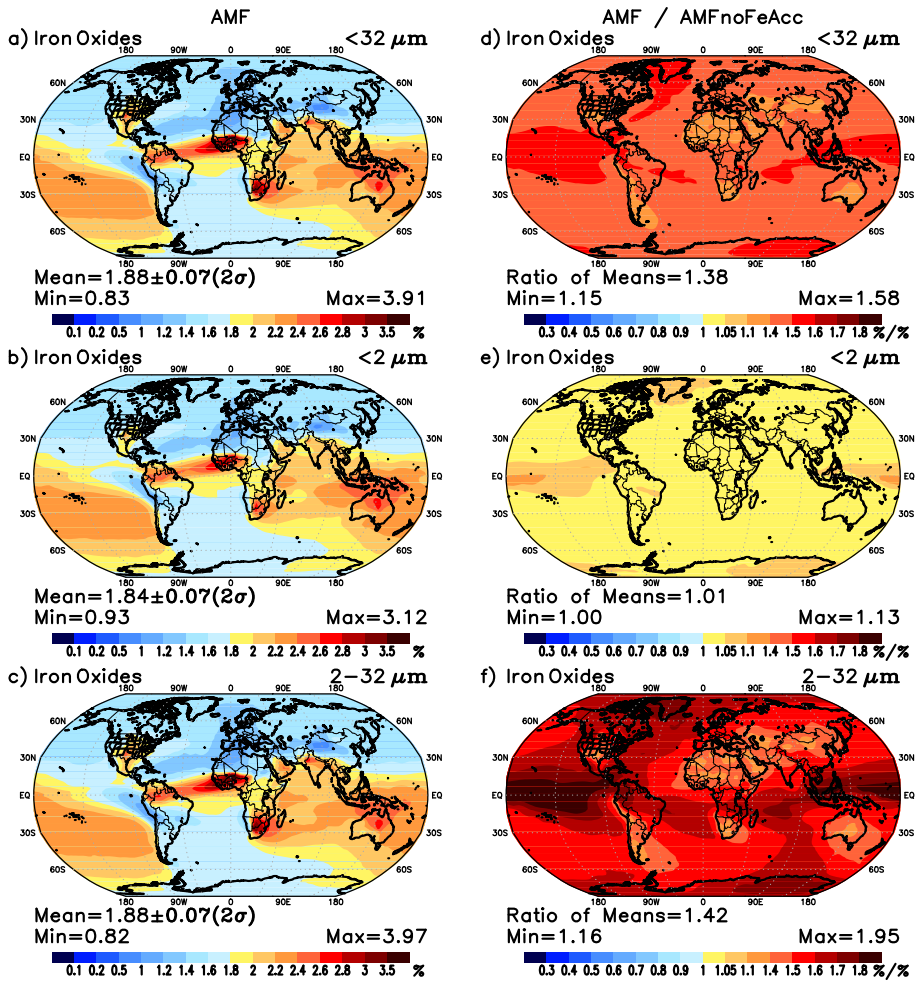


Figure S17. (Left panels) Annual-average column mass fraction of iron oxides for the aerosol mineral fraction (AMF) method and (right panels) ratio between the AMF method and the AMF method without iron oxide accretions (AMF-noFeAcc) for (a, d) total dust; (b, e) clay-sized dust, and (c, f) silt-sized dust.

3 Supplementary Tables

Table S1. Annual mean and standard deviation of dust cycle for the SMF and AMF method.

Variable	Size range	SMF	AMF
Emission [Tg a ⁻¹]	<i>Clay</i> (< 2 μm)	920 \pm 40	44 \pm 2
	<i>Silt</i> (2 – 16 μm)	657 \pm 30	1049 \pm 47
	<i>Silt</i> (16 – 32 μm)	647 \pm 30	1131 \pm 51
	<i>Total</i> (< 16 μm)	1577 \pm 70	1094 \pm 49
	<i>Total</i> (< 32 μm)	2224 \pm 100	2224 \pm 100
Load [Tg]	<i>Clay</i> (< 2 μm)	14.60 \pm 0.56	0.71 \pm 0.03
	<i>Silt</i> (2 – 16 μm)	4.66 \pm 0.17	7.31 \pm 0.26
	<i>Silt</i> (16 – 32 μm)	0.46 \pm 0.01	0.81 \pm 0.02
	<i>Total</i> (< 16 μm)	19.26 \pm 0.73	8.02 \pm 0.29
	<i>Total</i> (< 32 μm)	19.72 \pm 0.74	8.83 \pm 0.31
Wet deposition [Tg a ⁻¹]	<i>Clay</i> (< 2 μm)	652 \pm 29	31 \pm 1
	<i>Silt</i> (2 – 16 μm)	190 \pm 9	298 \pm 14
	<i>Silt</i> (16 – 32 μm)	14 \pm 3	25 \pm 5
	<i>Total</i> (< 16 μm)	842 \pm 37	330 \pm 16
	<i>Total</i> (< 32 μm)	856 \pm 39	355 \pm 20
Gravitational deposition [Tg a ⁻¹]	<i>Clay</i> (< 2 μm)	12 \pm 1	1 \pm 0.04
	<i>Silt</i> (2 – 16 μm)	357 \pm 19	576 \pm 30
	<i>Silt</i> (16 – 32 μm)	604 \pm 28	1054 \pm 48
	<i>Total</i> (< 16 μm)	369 \pm 20	577 \pm 30
	<i>Total</i> (< 32 μm)	973 \pm 48	1631 \pm 78
Turbulent deposition [Tg a ⁻¹]	<i>Clay</i> (< 2 μm)	239 \pm 14	12 \pm 1
	<i>Silt</i> (2 – 16 μm)	105 \pm 6	167 \pm 10
	<i>Silt</i> (16 – 32 μm)	29 \pm 2	51 \pm 3
	<i>Total</i> (< 16 μm)	344 \pm 20	179 \pm 10
	<i>Total</i> (< 32 μm)	373 \pm 22	230 \pm 13

References

- Kandler, K., Schütz, L., Deutscher, C., Ebert, M., Hofmann, H., Jäckel, S., Jaenicke, R., Knippertz, P., Lieke, K., Massling, A., Petzold, A., Schladitz, A., Weinzierl, B., Wiedensohler, A., Zorn, S., and Weinbruch,
75 S.: Size distribution, mass concentration, chemical and mineralogical composition and derived optical pa-
rameters of the boundary layer aerosol at Tinfou, Morocco, during SAMUM 2006, Tellus B, 61, 32–50,
doi:10.1111/j.1600-0889.2008.00385.x, <http://dx.doi.org/10.1111/j.1600-0889.2008.00385.x>, 2009.
- Perlitz, J. P., Pérez García-Pando, C., and Miller, R. L.: Predicting the mineral composition of dust aerosols.
Part I: Representing key processes, Atmos. Chem. Phys. Discuss., 15, 3493–3575, doi:10.5194/acpd-15-
80 3493-2015, <http://www.atmos-chem-phys-discuss.net/15/3493/2015/acpd-15-3493-2015.html>, 2015.
- Seinfeld, J. H. and Pandis, S. N.: Atmospheric Chemistry and Physics: From Air Pollution to Climate Change,
John Wiley & Sons, Inc., New York, 1998.